



Supercapacitor and Photocatalytic Applications of Hydrothermally Synthesized of Polydymite Nanoparticles

K.M. AJAY¹, M.N. DINESH¹, M. DHANALAKSHMI², M.N. SOMASHEKAR³, C.R. RAVIKUMAR^{4,*} and H.C. ANANDA MURTHY^{5,6,*}

¹Department of Electrical and Electronics Engineering, R.V. College of Engineering, Bengaluru-560059, India

²Department of Physics, Nrupathunga University (Formerly known as Government Science College), Bangalore-560001, India

³Department of Chemistry, S.S. Margol Degree College of Arts, Science and Commerce, Shahabad, Gulbarga (Dq)-585228, India

⁴Research Centre, Department of Chemistry, East West Institute of Technology, Bangalore-560091, India

⁵Department of Applied Sciences, Papua New Guinea University of Technology, Lae 411, Morobe Province, Papua New Guinea

⁶Department of Prosthodontics, Saveetha Dental College & Hospital, Saveetha Institute of Medical and Technical Science (SIMATS), Saveetha University, Chennai-600077, India

*Corresponding authors: E-mail: ravikumarcrc@ewit.edu.in; anandkps350@gmail.com

Received: 26 July 2024;

Accepted: 1 September 2024;

Published online: 30 September 2024;

AJC-21767

The hydrothermal technique for producing polydymite nanoparticles (Ni_3S_4 NPs) for photocatalytic and supercapacitor utilization is the main emphasis in present work. The microstructural and electrochemical characterizations were conducted to determine the performance parameters of supercapacitor such as specific capacitance, efficiency, energy density and power density values using cyclic voltammetric (CV) and electrochemical impedance spectroscopic (EIS) techniques. The electrochemical characteristics of Ni_3S_4 NPs were studied using a TMS electrode in a 2 M KOH solution. This showed a specific capacitance value of 524 F g^{-1} at a current density of 1 A g^{-1} . The Ni_3S_4 NPs showed good photocatalytic activities for the photodegradation of fast blue dye, the Ni_3S_4 NPs exhibits a 75.6% colour loss rate following the exposure for 120 min to UV radiation.

Keywords: Polydymite nanoparticles, Supercapacitors, Specific capacitance, Photocatalytic study, Fast blue dye.

INTRODUCTION

The supercapacitors may be thought of as a link between a standard capacitor and a battery or fuel cell device. As we know, the power density of a conventional capacitor is very high, which means that a conventional capacitor can discharge a small amount of charge in a short period of time, generating a lot of power, whereas the energy density of a battery device is very high, which means that a larger number of charges can be stored within the device for a slower discharge [1-3]. The supercapacitors and ultracapacitors are bang in the centre of them, with a significantly quicker discharge to provide more power while storing more charges. A supercapacitor is a high-capacity capacitor with a larger specific capacitance than normal capacitors but a lower voltage limit that bridges the gap between a rechargeable battery or fuel cell and an electrolytic capacitor. The supercapacitors are useful for multiple fast charge/discharge

cycles. It is typically not suggested or compatible with long-term compact energy storage systems such as autos, trains, elevators and so on [4-6].

There are two kinds of supercapacitors *e.g.* electrostatic double layer capacitors (EDLCs) and pseudocapacitors. EDLCs are composed of two carbon-based electrodes, an electrolyte and a separator. They operate on charge buildup principles and between the electrode and the electrolyte, there is no charge transfer. The primary idea is the accumulation of electrostatic charges over a double layer in case of EDLCs. The two layers avoid ion recombination. One downside of EDLCs is the need for a particular electrolyte dependent on the application [7,8]. Another issue to consider while using EDLCs is the electrode degradation. Metal oxide or conducting polymer electrodes are used in the pseudo capacitors. Unlike EDLCs, which store charges by electrostatic buildup between the electrodes, pseudo capacitors store charges *via* Faradic processes, which indicates

that a charge transfer occurs between the electrode and the electrolyte. Charge transfer occurs *via* electro-sorption, redox processes and the intercalation process. The pseudocapacitors can attain larger energy and power densities than EDLCs as well as higher specific capacitance, thanks to charge transfer *via* Faradic processes [9-11].

Water pollution has been a global concern in recent decades. The primary cause of this is the release of waste contaminants from manufacturing sectors that include food and medicines, as well as textile, cosmetic and plastics [12]. Water resources were seriously harmed by these enterprises, which produced around 8 to 9 lakh tons of dye annually and released 1 to 2 lakh tons into the environment, which had a variety of negative consequences on both human health and the ecosystem [13]. Approximately 4 million individuals every year pass away from severe poisoning as a result of these dyes [14]. Numerous treatment methods are currently available, including adsorption, ion exchange, filtration, flocculation and coagulation in addition to physical, chemical and biological therapy [15]. Unfortunately, the organic dyes cannot be entirely eliminated by any of these conventional treatment methods. Recent advancements in oxidation technologies, particularly photocatalytic degradation utilizing heterogeneous catalysts, have demonstrated potential for the mineralization of dyes into carbon dioxide and water [16]. Therefore, photocatalysis is a sustainable method that breaks down organic dyes from wastewater by working under UV light irradiation and generating degradable redox reactions.

Hybrid capacitors are often defined as a mix of EDLCs and pseudocapacitors. These capacitors are designed to take advantage of the respective benefits and minimize the relative shortcomings of EDLCs and pseudocapacitors. To perform charge and discharge operations, these capacitors employ both Faradic processes and electrostatic charge build-up. Hybrid capacitors have attained higher capacitances than EDLCs and pseudocapacitors during the last decade without sacrificing cyclic stability or cost [17,18]. The present work was proposed to synthesize polydymite nanoparticles (Ni_3S_4 NPs) for photocatalytic and electrode material for supercapacitor applications.

EXPERIMENTAL

The details of the chemicals used in this study along with their chemical name, molecular formula, molecular weight and physical properties are given in Table-1.

Stoichiometric calculations: The stoichiometric calculations to obtain the precursor solution, which undergoes the hydrothermal process. In brief, 2 g of nickel(II) chloride was mixed with 0.4377 g of sodium sulphide and 3.5 g of ascorbic

acid as reducing agent and dissolved in 80 mL distilled water to prepare the precursor solution.



Hydrothermal synthesis: Nickel chloride (2 g) was mixed with sodium sulphide (0.4377 g) and ascorbic acid (2 g) as reducing agent and dissolved in 80 mL of distilled water to prepare the precursor solution. This was transferred into a Teflon tube and the autoclave was closed and tightened. The autoclave was placed into the hot air oven and left at 180 °C for 20 h. The autoclave was cooled, solution transferred, centrifuged, dried and nanoparticles stored.

Preparation of electrode: After the synthesis of nanoparticles, the next step was fabrication of working electrodes for electrochemical testing. Firstly, weighed 85% of active materials and 10 wt.% of carbon black were transferred to mortar. Then 5% of N-methyl 2 pyrrolidone (NMP) and polyvinylidene fluoride (PVDF) were added to mortar containing TMS and carbon black to prepare the slurry. The prepared slurry was coated on 1 cm × 1 cm area of Toray carbon sheet on single side of sheet. The prepared electrodes were placed in the petri dish and dried in the hot air oven at 80 °C for 2 h to remove any moisture content present. The electrodes were tested for electrochemical properties using an electrochemical analyzer with three electrode systems. The role of carbon black was of a conducting material which on adding improves the conductivity by filling voids between particles. NMP was used as a solvent and PVDF as a binding agent because of its excellent chemical stability and wettability with electrolytes.

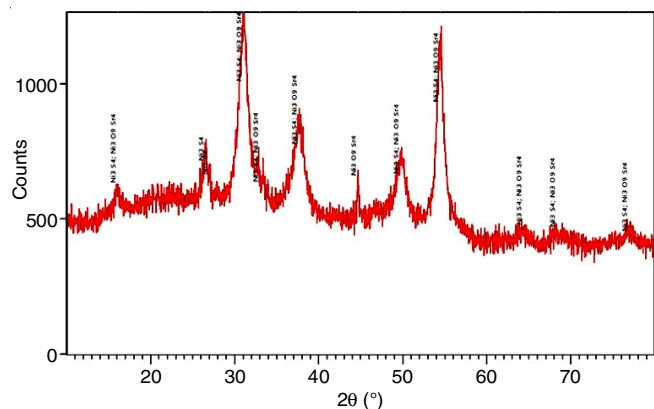
Characterization: The crystallinity of the samples was determined using the X-ray diffraction (XRD) technique (Diffract Plus V4, $\text{CuK}\alpha$ radiation). The surface morphology and surface topography were determined using the field emission scanning electron microscopy (FESEM) technique and the energy dispersive X-ray spectroscopy (EDX), respectively. A Shimadzu UV-visible spectrophotometer model 2600 was used to perform the photocatalytic activities.

RESULTS AND DISCUSSION

XRD studies: Fig. 1 displays the prepared polydymite nanoparticles (Ni_3S_4 NPs) powder diffraction (XRD) patterns. The XRD patterns of Ni_3S_4 compound shows distinct diffraction peaks at $2\theta = 16.06^\circ, 26.50^\circ, 27.033^\circ, 31.03^\circ, 33.05^\circ, 37.62^\circ, 44.64^\circ, 49.71^\circ, 54.45^\circ, 64.30^\circ, 68.33$ and 6.90° . All of the XRD patterns corresponded perfectly with the JCPDS card number JCPDS 47-1739 and the cubic phase [19].

TABLE-1
DESCRIBES ALL THE CHEMICALS UTILIZED THE PROJECT WITH THEIR CHEMICAL NAME, MOLECULAR FORMULA AND MOLECULAR WEIGHT

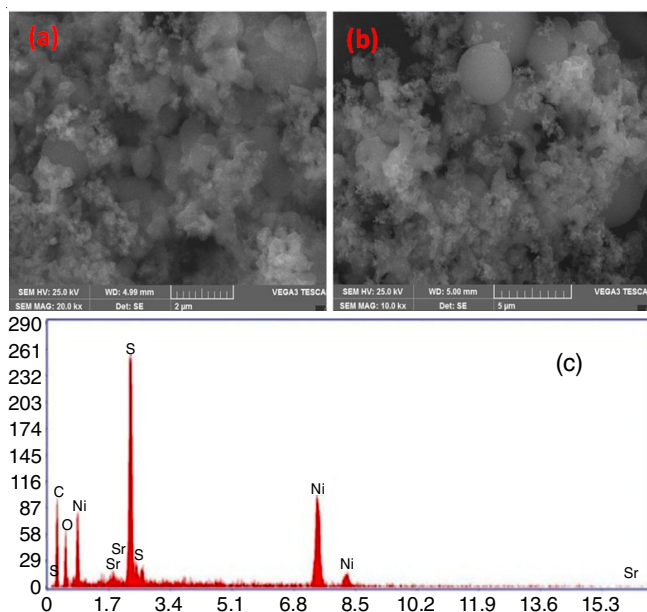
| Chemical name | m.f. | m.w. (g/mol) | Properties |
|--------------------------------|---|-----------------|--|
| Nickel(II) chloride | $\text{NiCl}_2 \cdot 6\text{H}_2\text{O}$ | 237.69 | Appearance: Green crystals; density: 1.92 g/cm ³ ; m.p.: 140 °C; highly hygroscopic |
| Sodium sulphide | Na_2S | 78 | Appearance: Yellow crystals; density: 1.856 g/cm ³ ; m.p.: 1,176 °C; anhydrous |
| Ascorbic acid (Reducing agent) | – | – | Natural reducing agent (vitamin C) |
| Pure distilled water | H_2O | 18 | De-ionized water obtained from chemistry laboratory |

Fig. 1. XRD pattern of Ni_3S_4 NPs

Morphological studies: The SEM image of Ni_3S_4 NPs sample exhibits the hexapod like structures (Fig. 2a-b). Fig. 2a shows the SEM image of Ni_3S_4 at a magnification of $5\ \mu\text{m}$, which gives the insight of high specific surface area of the compound for deposition. While the SEM image in Fig. 2b at the magnification of $2\ \mu\text{m}$ and the Ni_3S_4 sample indicate a tightly packed arrangement of molecules with uneven sizes, further describing the microstructure. The 3D architecture of the synthesized polydymite nanoparticles helps to improve its specific area, which speeds up the absorption of electrons that were transferred during the electrode reactions. The EDX spectrum (Fig. 2c) of Ni_3S_4 NPs exhibits the main components were nickel, sulphur, carbon and oxygen. At energy line of 8.5 keV, the characteristics of nickel and sulphur are visible.

Fig. 3a-b shows the TEM micrographs of the prepared Ni_3S_4 NPs. Using Origin and Image J software, the particle size of the produced Ni_3S_4 NPs was determined to be 38 nm. This matched with the PXRD values almost exactly and also revealed the agglomeration of nanoparticles. The unique ring patterns were observed in the selected area of the electron diffraction (SAED) pattern, as shown in Fig. 3c, which verifies their polycrystalline nature and every circle matched the (hkl) planes of the PXRD.

Electrochemical characterization: All the CV, GCD and EIS measurements were carried out utilizing a three-electrode system in a 2 M KOH electrolyte in order to examine the electrochemical performances of the electrode materials.

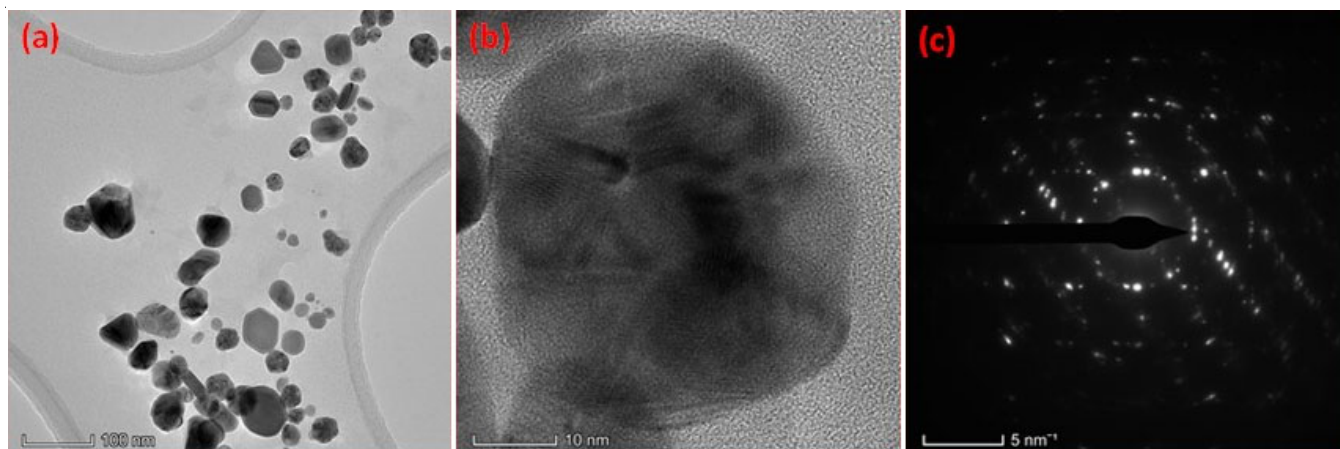
Fig. 2. SEM (a-b) and EDX (c) images of Ni_3S_4 NPs at different magnifications

Cyclic voltammetry: Fig. 4 shows the cyclic voltammograms of Ni_3S_4 NPs under a potential window of 0-0.55 V (vs. Hg/HgO) at scan rates of 2, 5, 10, 50, 70, 90 and 100 mV/s. The reversible Faradaic redox reactions occurring within the electroactive materials provide the distinctive pseudocapacitive features to the CV curves. The electrochemical capacitance of Ni_3S_4 , which is believed to be mediated by OH^- ions in alkaline electrolyte, is thus mainly caused by the $\text{Ni}^{2+}/\text{Ni}^{3+}$ redox pair. Furthermore, even at a high scanning rate of 100 mV/s, the anodic and cathodic peaks are comparable, indicating good rate capability. As shown in Fig. 4, the galvanostatic charge-discharge curves were remeasured.

Using eqn. 6, the C_s (specific capacitance) standards of the Ni_3S_4 electrode were obtained from eqn. 2 [20]:

$$C_s = Q \cdot m \cdot \Delta V \quad (2)$$

where C_s = specific capacitance, Q = cathodic/anodic charges on each scanning, m = electroactive material mass and ΔV = potential window. At a scan rate 1 mV/s, the specific capacitance can reach a maximum of 524.96 F/g.

Fig. 3. (a) TEM images, (b) HRTEM and (c) SAED pattern of Ni_3S_4 NPs

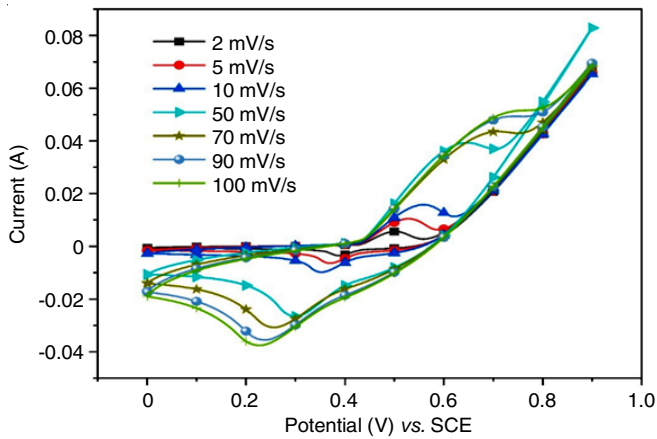


Fig. 4. Cyclic voltammogram of Ni₃S₄ electrode at different scan rate vs. Hg/HgO electrode

Exploring the electrochemical characteristics at the interface of Ni₃S₄ electrode using electrochemical impedance spectroscopy (EIS) (Fig. 5). At high frequencies, the current response showed a semi-circular zone whose diameter was equal to the charge transfer resistance (R_{ct}), suggesting that the process was limited by electron transfer. Significantly, the Ni₃S₄ electrode demonstrated a lower R_{ct} , suggesting diminished electron resistance [21]. This decrease in electron transfer resistance after the modification could be attributed to the improved electron transfer properties as indicated in Table-2 obtained from fitted circuit (inset of Fig. 5).

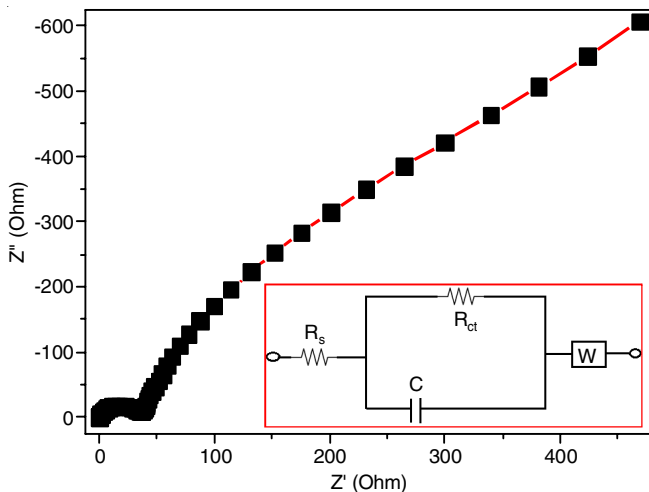


Fig. 5. Electrochemical impedance spectra of Ni₃S₄ electrode with fitted circuit

| TABLE-2 CHARGE TRANSFER RESISTANCE AND CAPACITANCE VALUES OF Ni ₃ S ₄ ELECTRODE MATERIAL | | | |
|---|--------------------|-----------------------|-------------------------|
| Sample | R_s (Ω) | R_{ct} (Ω) | $C_{dl} \times 10^{-5}$ |
| Ni ₃ S ₄ electrode | 15.4 | 42.5 | 2.55 |

Galvanostatic charge/discharge: Fig. 6 shows the relation between potential and time. Moreover, the Ni₃S₄ molecule is thought to promote quick redox reactions and brief electron and ion diffusion pathways. By applying eqn. 3, the capacitance at each electrode was determined [21].

$$C = \frac{i \cdot \Delta t}{m \Delta V} \tag{3}$$

where i , ΔV , Δt and m represent the applied currents, potential range, time of a discharge cycle and mass of Ni₃S₄ electrode, respectively. At a current density as high as 20 A g⁻¹, the Ni₃S₄ electrode keeps 20% capacity retention (90.90 F g⁻¹). The specific capacitances of Ni₃S₄ electrode were estimated to be 524.96, 423.29, 369.84, 331.65, 301.81, 276, 253.26, 234.12, 216, 203.63, 174.54, 139.09, 111.27 and 90.90 F g⁻¹ at current densities of 1, 2, 3, 4, 5, 6, 7, 8, 9, 10, 12, 15, 18 and 20 A g⁻¹, respectively. The specific capacitances show a reduction with increasing current density, potentially because of a short Faradic redox reaction time at high discharge rates. At a constant current density of 1.0 A g⁻¹, the specific capacitance values with respect to cycle numbers are determined in order to assess the stability of Ni₃S₄ electrode (Fig. 7). After the first 100 cycles, there was a modest decline in the specific capacitance and after 2000 cycles, 85% of the initial specific capacitance is still present. This high degree of stability indicates that the nickel sulphide electrode and electrolyte underwent a reversible surface redox reaction.

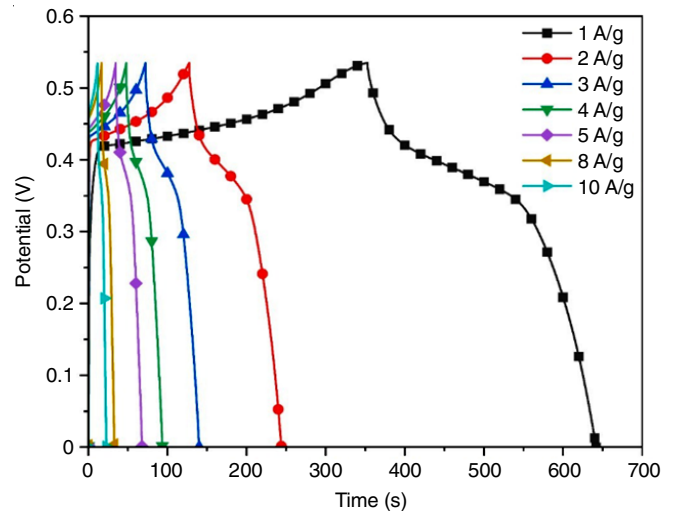


Fig. 6. Charge discharge curve of Ni₃S₄ electrode at various current densities

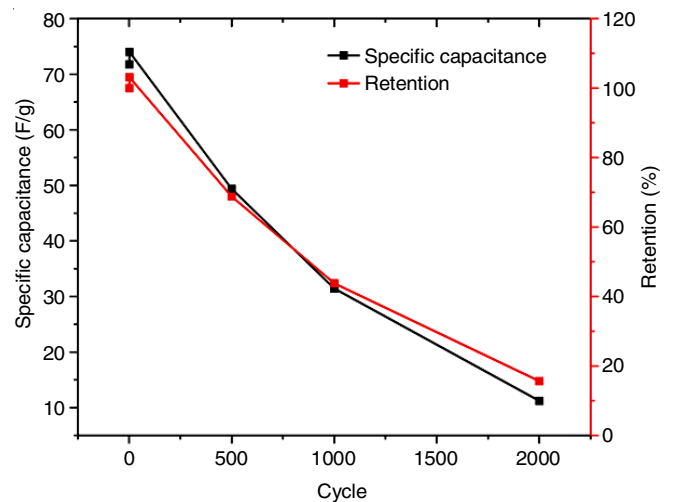


Fig. 7. Specific capacitance as a function of cycle numbers

In this work, the photocatalytic studies were carried out and found that Ni₃S₄ nanomaterial as photocatalyst under UV light exhibits the maximum emission intensity. The Ni₃S₄ NPs were employed in a photocatalytic experiment to degrade the chosen dye, fast blue, in the presence of UV light. The 400 W mercury lamp with a wavelength of 254 nm was used to light the reaction mixture while it was being magnetically agitated. After being exposed to UV light for 120 min in the open air, 5 mL of sample solution were removed from the reaction mixture and observed in the UV-visible range of 200-800 nm at 15 min intervals. Fast blue dye (60 mg) was added to 20 ppm solutions of the catalyst for 120 min, the dye was exposed to UV radiation [22,23].

The maximum absorbance peak of fast blue dye was observed at 613 nm under UV light as shown in Fig. 8a. The absorbance peaks steadily reduced with the irradiation period when the solution was exposed to UV light ($\lambda = 254$ nm) in the presence of Ni₃S₄ photocatalyst, indicating the photocatalytic capacity of Ni₃S₄ NPs [24,25]. At the beginning, the absorption peak for fast blue dye decreased rapidly and it slowed down gradually until equilibrium was attained. Since there were so many active sites on the catalyst, the first phase of adsorption happened quickly. However, after a while, the occupancy of these sites made adsorption less effective [26].

The photocatalytic efficiency of hydrothermal synthesized Ni₃S₄ NPs was studied and degradation percentage of dye was calculated as 75.6% under UV light for fast blue dye irradiated for 120 min as shown in Fig. 8b [27,28]. The percentage of degradation was calculated by using eqn. 4:

$$\text{Degradation (\%)} = \frac{C_o - C_t}{C_e} \times 100 \quad (4)$$

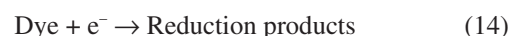
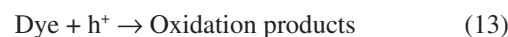
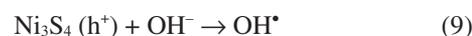
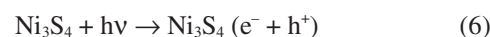
where C_e and C_t are the concentration of dye at equilibrium at time t , respectively [24]. To study degradation kinetics of dye, the pseudo-first-order kinetics model (eqn. 5) was applied.

$$\ln\left(\frac{C_o}{C_t}\right) = -Kt \quad (5)$$

where C_0 is the initial concentration of aqueous fast blue dye solution after achieving an adsorption-desorption equilibrium with photocatalyst; C_t is the fast blue dye concentration at a given irradiation time in the system and k is the apparent rate constant [25,29]. The plot of C/C_0 vs. irradiation time for Ni₃S₄ NPs photocatalyst is displayed in Fig. 8c.

Mechanism: Based on the previous explanation, the improved photocatalytic activity of mechanism of fast blue dye mechanism is shown in Fig. 9, whereby the recombination of photogenerated electron-hole pairs is inhibited. The sun rays cause the fast blue molecules to produce holes, photoelectron volts and conduction bands in turn. When oxygen, either in a dissolved form or adsorbed on a surface, reacts with the photogenerated electrons carried to the fast blue dye, superoxide is produced. The excess holes on the valence band remain in fast blue dye and react with H₂O and OH⁻ to form active substances such as OH[•]. The fast blue dye is then degraded by photocatalysis, which is then carried out *via* a well-known mechanism of visible light-driven electron emission from the valence band to the conduction band and the generation of oxidative intermediate species, O₂^{•-} and [•]OH [30-34].

The steps involved in the photocatalytic degradation process under UV light irradiation are as follows:



Conclusion

The synthesis of polydymite nanoparticles (Ni₃S₄ NPs) was carried out by hydrothermal method with the reaction temperature and time being 180 °C and 20 h, respectively using non-toxic chemicals like ascorbic acid and water. The obtained Ni₃S₄ nanomaterials were subjected to the microstructural and electrochemical studies. Their electrochemical performance in a 2 M KOH electrolyte was then investigated. The PXRD pattern of Ni₃S₄ nanomaterials revealed a typical cubic phase. Electrochemical investigations, such as cyclic voltammetry, AC impedance, and galvanostatic charge-discharge, were

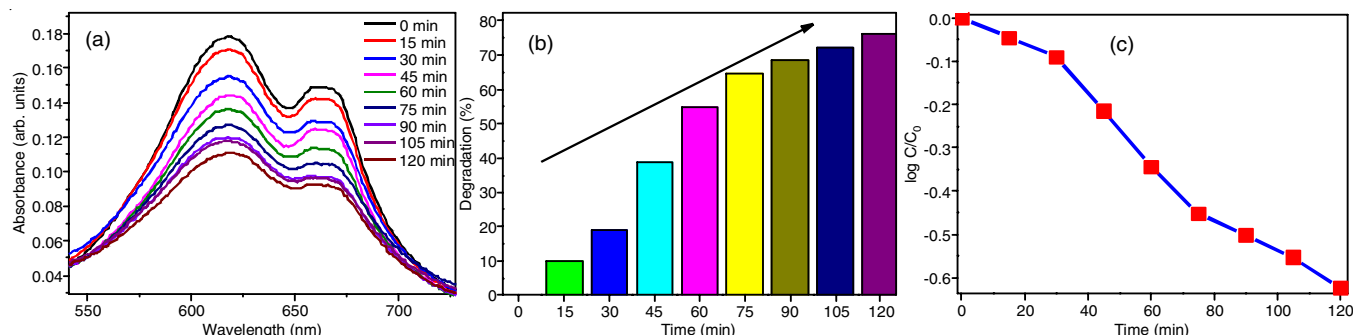


Fig. 8. (a) Absorbance spectra of Ni₃S₄ photocatalyst for decolorization of fast blue dye under UV illumination, (b) Degradation percentage of fast blue dye with time and (c) Plot of C/C_0 vs. irradiation time for fast blue photocatalyst

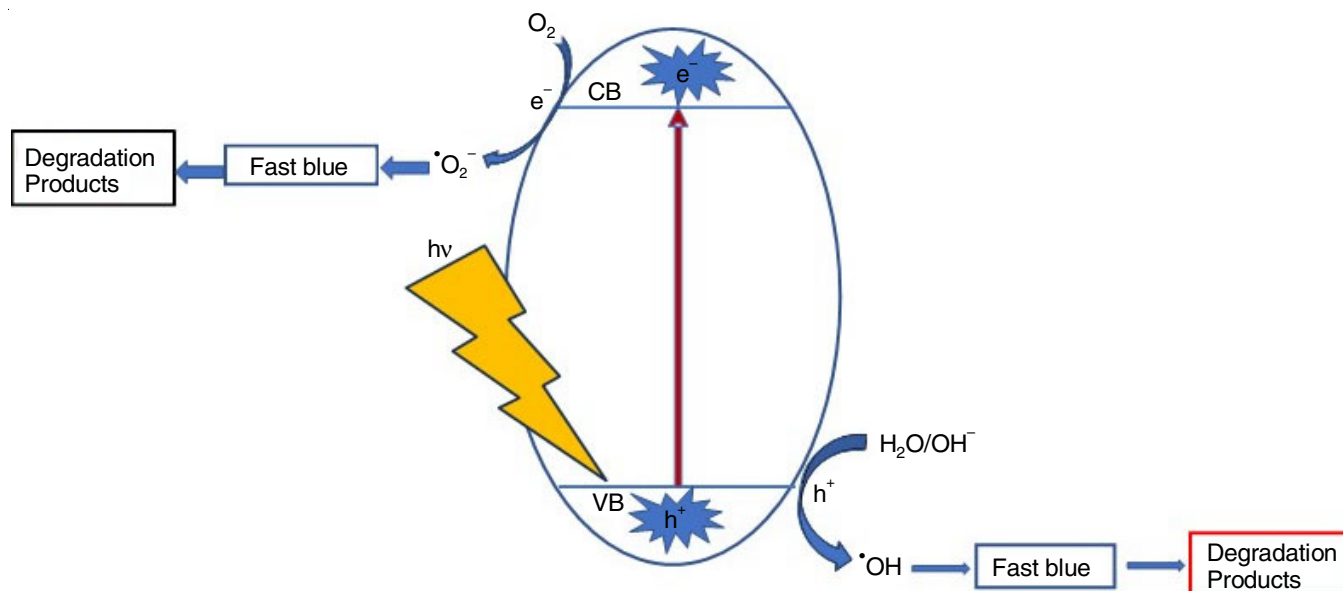


Fig. 9. Proposed mechanism for the photocatalytic degradation of fast blue dye under UV light irradiation

conducted using electrodes constructed from the synthesized nanomaterials. The Ni_3S_4 NPs confirmed the occurrence of oxidation and reduction of the material during the electrochemical analysis for different scan rates from 2-100 mV/s. After 2000 cycles, almost 85% of initial capacity was still there, demonstrating impressive cycling stability. Under UV light, the Ni_3S_4 NPs exhibited an impressive photodegradation performance of 75.6% 120 min against the fast blue dye. The results indicated that the prepared Ni_3S_4 NPs could be useful materials for wastewater treatment and supercapacitor applications.

ACKNOWLEDGEMENTS

The authors are grateful to the management of Rashtreeya Sikshana Samithi Trust (RSST), The Principal and HOD (Department of Electrical and Electronics Engineering), R V College of Engineering, Bangalore, India for overall support and generous encouragement.

CONFLICT OF INTEREST

The authors declare that there is no conflict of interests regarding the publication of this article.

REFERENCES

- J. Sun, B. Luo and H. Li, *Adv. Energy Sustain. Res.*, **3**, 2100191 (2022); <https://doi.org/10.1002/aesr.202100191>
- M. Czagany, S. Hompoth, A.K. Keshri, N. Pandit, I. Galambos, Z. Gacsi and P. Baumli, *Materials*, **17**, 702 (2024); <https://doi.org/10.3390/ma17030702>
- M. Yassine and D. Fabris, *Energies*, **10**, 1340 (2017); <https://doi.org/10.3390/en10091340>
- J. Qu, Y. Bai, X. Li, K. Song, S. Zhang, X. Wang, X. Wang and S. Dai, *J. Mater. Res. Technol.*, **15**, 6155 (2021); <https://doi.org/10.1016/j.jmrt.2021.11.036>
- A.K. Nayak, A.K. Das and D. Pradhan, *ACS Sustain. Chem. Eng.*, **5**, 10128 (2017); <https://doi.org/10.1021/acssuschemeng.7b02135>
- Y. Zheng, Y. Tian, S. Sarwar, J. Luo and X. Zhang, *J. Power Sources*, **452**, 227793 (2020); <https://doi.org/10.1016/j.jpowsour.2020.227793>
- J. Yang, Z. Sun, J. Wang, J. Zhang, Y. Qin, J. You and L. Xu, *CrystEngComm*, **21**, 994 (2019); <https://doi.org/10.1039/C8CE01805G>
- A. Chang, C. Zhang, Y. Yu, Y. Yu and B. Zhang, *ACS Appl. Mater. Interfaces*, **10**, 41861 (2018); <https://doi.org/10.1021/acsami.8b16072>
- K. Guo, F. Yang, S. Cui, W. Chen and L. Mi, *RSC Adv.*, **6**, 46523 (2016); <https://doi.org/10.1039/C6RA06909F>
- G. Zhang, H. Xuan, J. Yang, R. Wang, Z. Xie, X. Liang, P. Han and Y. Wu, *J. Power Sources*, **506**, 230255 (2021); <https://doi.org/10.1016/j.jpowsour.2021.230255>
- J. Zhang, H. Feng, J. Yang, Q. Qin, H. Fan, C. Wei and W. Zheng, *ACS Appl. Mater. Interfaces*, **7**, 21735 (2015); <https://doi.org/10.1021/acsami.5b04452>
- C.H. Liao, C.W. Huang and J.C.S. Wu, *Catalysts*, **2**, 490 (2012); <https://doi.org/10.3390/catal2040490>
- M.A. Al-Ghouti, M.A. Khrasheh, S.J. Allen and M.N. Ahmad, *J. Environ. Manage.*, **69**, 229 (2003); <https://doi.org/10.1016/j.jenvman.2003.09.005>
- P.H. Borse, H. Jun, S.H. Choi, S.J. Hong and J.S. Lee, *Appl. Phys. Lett.*, **93**, 173103 (2008); <https://doi.org/10.1063/1.3005557>
- Y. Tamaura, Y. Ueda, J. Matsunami, N. Hasegawa, M. Nezuaka, T. Sano and M. Tsuji, *Sol. Energy*, **65**, 55 (1999); [https://doi.org/10.1016/S0038-092X\(98\)00087-5](https://doi.org/10.1016/S0038-092X(98)00087-5)
- C.H. Li, K.C.K. Soh and P. Wu, *J. Alloys Compd.*, **372**, 40 (2004); <https://doi.org/10.1016/j.jallcom.2003.10.017>
- A. Muzaffar, M.B. Ahamed, K. Deshmukh and J. Thirumalai, *Renew. Sustain. Energy Rev.*, **101**, 123 (2019); <https://doi.org/10.1016/j.rser.2018.10.026>
- P.E. Lokhande, U.S. Chavan and A. Pandey, *Electrochem. Energy Rev.*, **3**, 155 (2020); <https://doi.org/10.1007/s41918-019-00057-z>
- C. An, Z. Zhang, X. Chen and Y. Liu, *Mater. Lett.*, **60**, 3631 (2006); <https://doi.org/10.1016/j.matlet.2006.03.073>
- V.G.D. Kumar, K.R. Balaji, R. Viswanatha, G. Ambika, R. Roopa, B.M. Basavaraja, M. Chennabasappa, C.R.R. Kumar, Z. Chen, X.-T. Bui and M.S. Santosh, *Chemosphere*, **287**, 132174 (2022); <https://doi.org/10.1016/j.chemosphere.2021.132174>
- R.L. Naik, T.B. Narsaiah, P. Justin, A.N. Kumar, M.N. Somashekar, N. Raghavendra, C.R. Ravikumar, A.A. Khan and M.S. Santosh, *Mater. Sci. Eng. B*, **298**, 116861 (2023); <https://doi.org/10.1016/j.mseb.2023.116861>

22. D. Matei, A.U. Katsina, S. Mihai, D.L. Cursaru, R. Somoghi and C.L. Nistor, *Polymers*, **15**, 1210 (2023); <https://doi.org/10.3390/polym15051210>
23. J. Cao, S. Sun, X. Li, Z. Yang, W. Xiong, Y. Wu, M. Jia, Y. Zhou, C. Zhou and Y. Zhang, *Chem. Eng. J.*, **382**, 122802 (2020); <https://doi.org/10.1016/j.cej.2019.122802>
26. N.N. Ahamed, M.R. Anil Kumar, N. Raghavendra, T.M. Sharanakumar, J. Pattar, N. Basavaraju, C.R. Ravikumar and H.C.A. Murthy, *RSC Adv.*, **14**, 17664 (2024); <https://doi.org/10.1039/D4RA01706D>
27. C.Y. Cao, Z.M. Cui, C.Q. Chen, W.G. Song and W. Cai, *J. Phys. Chem. C*, **114**, 9865 (2010); <https://doi.org/10.1021/jp101553x>
28. S.L. Zhong, L.F. Zhang, L. Wang, W.X. Huang, C.M. Fan and A.W. Xu, *J. Phys. Chem. C*, **116**, 13127 (2012); <https://doi.org/10.1021/jp3017826>
24. Q. Zhang, K. Zhang, D. Xu, G. Yang, H. Huang, F. Nie, C. Liu and S. Yang, *Prog. Mater. Sci.*, **60**, 208 (2014); <https://doi.org/10.1016/j.pmatsci.2013.09.003>
25. B.K. Meyer, A. Polity, D. Reppin, M. Becker, P. Hering, P.J. Klar, Th. Sander, C. Reindl, J. Benz, M. Eickhoff, C. Heiliger, M. Heinemann, J. Bläsing, A. Krost, S. Shokovets, C. Müller and C. Ronning, *Phys. Status Solidi, B Basic Res.*, **249**, 1487 (2012); <https://doi.org/10.1002/pssb.201248128>
29. E. Guo and L. Yin, *Phys. Chem. Chem. Phys.*, **17**, 563 (2015); <https://doi.org/10.1039/C4CP03132F>
30. Z. Zhang, K. Liu, Y. Bao and B. Dong, *Appl. Catal. B*, **203**, 599 (2017); <https://doi.org/10.1016/j.apcatb.2016.10.064>
31. M.U. Anu Prathap, B. Kaur and R. Srivastava, *J. Colloid Interface Sci.*, **370**, 144 (2012); <https://doi.org/10.1016/j.jcis.2011.12.074>
32. S. Zaman, A. Zainelabdin, G. Amin, O. Nur and M. Willander, *J. Phys. Chem. Solids*, **73**, 1320 (2012); <https://doi.org/10.1016/j.jpcs.2012.07.005>
33. S. Liu, J. Tian, L. Wang, Y. Luo and X. Sun, *Catal. Sci. Technol.*, **2**, 339 (2012); <https://doi.org/10.1039/C1CY00374G>
34. W. Shi and N. Chopra, *ACS Appl. Mater. Interfaces*, **4**, 5590 (2012); <https://doi.org/10.1021/am301488c>